The structure of the D49 phospholipase A$_2$ piratoxin III from *Bothrops pirajai* reveals unprecedented structural displacement of the calcium-binding loop: possible relationship to cooperative substrate binding

Daniel J. Rigden,[a]***** **Lee When Hwa,**[b]**†** **Sérgio Marangoni,**[c] **Marcos H. Toyama**[c] **and Igor Polikarpov**[b,d]

[a]Embrapa Recursos Genéticos e Biotecnologia, Cenargen/Embrapa, Brasília, DF, Brazil, [b]Laboratório Nacional de Luz Síncrotron, Campinas, SP, Brazil, [c]Departamento de Bioquímica, Instituto de Biologia, UNICAMP, Campinas, SP, Brazil, and [d]Grupo de Cristalografia, Departamento de Física de São Carlos, Universidade de São Paulo, São Carlos, SP, Brazil

† Present address: Computational Biology and Bioinformatics, Department of Molecular Biology TPC-28, The Scripps Research Institute, La Jolla, CA, USA.

Correspondence e-mail:
daniel@cenargen.embrapa.br

Snake venoms are rich sources of phospholipase A$_2$ homologues, both active calcium-binding Asp49 enzymes and essentially inactive Lys49 proteins. They are responsible for multiple pharmacological effects, some of which are dependent on catalytic activity and others of which are not. Here, the 2.4 Å X-ray crystal structure of an active Asp49 phospholipase A$_2$ from the venom of the snake *Bothrops pirajai*, refined to conventional and free R values of 20.1 and 25.5%, respectively, is reported. Unusually for phospholipases A$_2$, the dependence of the enzyme rate on the substrate concentration is sigmoidal, implying cooperativity of substrate binding. The unprecedented structural distortion seen for the calcium-binding loop in the present structure may therefore be indicative of a T-state enzyme. An explanation of the interaction between the substrate-binding sites based on the canonical phospholipase A$_2$ dimer is difficult. However, an alternative putative dimer interface identified in the crystal lattice brings together the calcium-binding loops of neighbouring molecules, along with the C-terminal regions which are disulfide bonded to those loops, thereby offering a possible route of communication between active sites.

1. Introduction

Phospholipases A$_2$ (PLA$_2$s; E.C. 3.1.1.4) catalyse the specific hydrolysis of the *sn*-2 acyl bond of *sn*-3 phospholipids, producing lysophospholipids and fatty acids. The best understood phospholipase A$_2$ family encompasses enzymes from mammals, insects and snakes. The first structural determination of a member of this major family was that of the bovine pancreatic enzyme (Dijkstra *et al.*, 1978). Interest in the enzymes from mammalian sources has focused recently on the potential of their inhibitors as anti-inflammatory agents (*e.g.* Schevitz *et al.*, 1995). Crystal structures of PLA$_2$s from snakes (*e.g.* Keith *et al.*, 1981) and insects (Scott *et al.*, 1990) have showed them to have an evolutionary relationship with the bovine pancreatic enzyme. These enzymes share a functional dependence on a Ca^{2+} ion, which binds to Asp49 (bovine pancreatic enzyme numbering) and three backbone carbonyl groups in the 'calcium-binding loop', and a conserved catalytic machinery centred on His48. Sequence and structural comparisons (*e.g.* Scott & Sigler, 1994) have enabled the division of the group into three classes: the highly homologous classes I and II and a more varied class III. The structure of the evolutionarily distinct human cytosolic enzyme has recently been determined and represents the first class IV PLA$_2$ structure (Dessen *et al.*, 1999).

Table 1
Crystal and data statistics.

Values in parentheses are for the highest resolution shell.

Space group	$C2$
Unit-cell parameters (Å, °)	$a = 61.0$, $b = 100.9$, $c = 48.3$, $\beta = 123.8$
Resolution (Å)	14.7–2.4 (2.5–2.4)
Completeness (%)	85.9 (89.6)
$\langle I/\sigma(I)\rangle$	7.3 (2.1)
Average redundancy	2.88 (2.0)
R_{merge} (%)	11.4 (26.4)

Snake venoms are remarkable for containing multiple PLA_2 homologues (Pan *et al.*, 1998; Tsai *et al.*, 2000) with different pharmacological properties, among them myotoxicity (Gutierrez & Lomonte, 1995), oedema formation (Lloret & Moreno, 1993), neurotoxicity (Verity, 1992) and platelet aggregation (Gerrard *et al.*, 1993). Many of these properties are conferred by regions of the structure not involved in catalysis, as illustrated by the myotoxicity of the minimally catalytically active (*e.g.* Shimohigashi *et al.*, 1995) subgroup of PLA_2 homologues which possess a lysine at position 49 (Maraganore *et al.*, 1984). Numerous attempts have been made to correlate their sequence and structural characteristics with their pharmacological properties (*e.g.* Ward *et al.*, 1998).

Three PLA_2 homologues derived from the venom of the snake *Bothrops pirajai* have been the subjects of biochemical (Toyama *et al.*, 1999, 2000; Soares *et al.*, 2001) and crystallographic studies (Lee *et al.*, 2001). Piratoxins I and II, with near-identical sequences (Toyama *et al.*, 2000), are essentially inactive Lys49 PLA_2 homologues, while piratoxin III is an active Asp49 PLA_2 enzyme (Mancuso *et al.*, 1995; Soares *et al.*, 2001) identical to the separately sequenced MP-III 4R (Toyama *et al.*, 1999).

Here, we present a crystal structure of piratoxin III. In common with several other PLA_2s (Burke *et al.*, 1995; Beghini *et al.*, 2000), piratoxin III exhibits a cooperative relationship between enzyme rate and substrate concentration. The structure contains a dramatically distorted Ca^{2+}-binding loop and may represent an inactive T-state of the enzyme.

2. Materials and methods

2.1. Protein purification

PrTX-III was isolated and purified from the whole venom of *B. pirajai* by reverse-phase and cation-exchange HPLC. 20 mg of whole venom were dissolved in 250 µl 0.1%(*v/v*) trifluoro-acetic acid (solvent *A*). The resulting sample was centrifuged and the supernatant was applied onto a 0.78 × 30 cm μ-Bondapack C-18 column (Waters 991 – PDA system).

Purification of the venom was performed with a linear gradient of 0–66%(*v/v*) acetonitrile in 0.1%(*v/v*) trifluoro-acetic acid (solvent *B*) at a flow rate of 2.0 ml min^{-1} and was monitored at 280 nm. The MPIII fraction was lyophilized and dissolved in 0.05 *M* ammonium bicarbonate pH 7.4, centrifuged and applied onto a 0.39 × 7.8 cm protein pack SP 5PW cation-exchange column previously equilibrated with the same buffer. Elution of PrTX-III was performed using a linear gradient of ammonium bicarbonate from 0.05 to 1.0 *M* at pH 7.4. The chromatographic run was performed at flow rate of 1.0 ml min^{-1} and was monitored at 280 nm. The purified sample was lyophilized and used for crystallization trials.

2.2. Crystallization and collection of X-ray diffraction data

Preliminary screening for crystallization conditions was performed using a sparse-matrix screen at 291 K (Crystal Screens I and II, Hampton Research). Lyophilized PrTX-III was initially dissolved in water to a concentration of 10 mg ml^{-1} and used in the screening procedure. Small crystals were found using solution 40 of the Crystal Screen I kit (20% 2-propanol, 20% PEG 4000, 0.1 *M* sodium citrate pH 5.6). These conditions were then refined. Plate-like crystals measuring 0.1 × 0.1 × 0.02 mm were grown at 291 K using the hanging-drop vapour-diffusion method by mixing equal volumes (1 µl + 1 µl) of a protein solution concentrated to 5 mg ml^{-1} with a reservoir solution consisting of 18% 2-propanol, 21% PEG 4000 and 0.1 *M* sodium citrate pH 5.3. Crystals appeared in 10–15 d.

X-ray diffraction data were collected at the Protein Crystallography beamline (Polikarpov *et al.*, 1998) at the Laboratório Nacional de Luz Síncrotron (LNLS), Campinas, Brazil. The images were recorded on a MAR345 image plate using synchrotron radiation at an optimal wavelength of 1.535 Å (Polikarpov *et al.*, 1997). The images were processed and scaled with the *DENZO* and *SCALEPACK* programs (Otwinowski, 1993), yielding the statistics in Table 1. Calculations of Matthews coefficients (Matthews, 1968) suggested the presence of two molecules per asymmetric unit ($V_M = 2.84$ Å^3 Da^{-1}).

2.3. Computational crystallographic methods

MOLREP (Vagin & Teplyakov, 1997) was used to solve the structure by molecular replacement. Crystallographic refinement then proceeded with alternating rounds of computational refinement and map calculation with *CNS* (Brünger *et al.*, 1998) and manual model inspection and modification with *O* (Jones *et al.*, 1991). A free *R* factor (Brünger, 1992), calculated from 5% of reflections set aside at the outset, was used to monitor the progress of refinement, to aid in the choice of *B*-factor refinement protocol at different stages of refinement and to help choose appropriate schemes for handling non-crystallographic symmetry (Kleywegt & Brünger, 1996). In this way, the initial anisotropic overall *B* factor was replaced successively with per-residue *B* factors, separate per-residue *B* factors for main- and side-chain atoms and, finally, restrained individual atomic *B* factors. Initial refinement was carried out using a strict NCS relationship between the two monomers in the asymmetric unit. When refinement under this scheme could proceed no further, it was replaced by a system of strong restraints on both coordinates and *B* factors, from which NCS-breaking residues were progressively exempted based on examination of maps.

Table 2
Initial refinement based on different starting models.

PDB structure used to build model	Rigid-body refinement	R_{free} values after Torsion-angle simulated annealing		
		Maximum	Minimum	Mean
1aok	0.510	0.483	0.458	0.469
1b4w	0.509	0.439	0.415	0.431
1cl5	0.507	0.423	0.386	0.410
1clp	0.515	0.454	0.426	0.441
1vip	0.503	0.483	0.439	0.453

The model bias present in the initial molecular-replacement solution was tackled using σ_A-weighted electron-density maps (Read, 1986), maximum-likelihood refinement targets (Pannu & Read, 1996), torsion-angle simulated annealing (Rice & Brünger, 1994; Adams *et al.*, 1997) and solvent flattening (Cowtan & Zhang, 1999). All data in the 15 to 2.4 Å resolution range were used throughout, without the application of σ or amplitude-based cutoffs. A variety of stereochemical (Laskowski *et al.*, 1993) and other analyses (Jones *et al.*, 1991; Kleywegt & Jones, 1996) were periodically performed in order to locate possible model errors. Coordinate, topology and parameter files for 2-propanol were obtained from the HIC-UP database (Kleywegt & Jones, 1998). When the free R value reached 27%, waters were added in three cycles using programs from the *CCP*4 package (Collaborative Computational Project, Number 4, 1994). Water molecules were placed into 3σ peaks in σ_A-weighted $F_o - F_c$ maps when they were within a suitable hydrogen-bonding distance of the existing model. After refinement, water molecules whose positions were not supported by electron density at 1σ contouring in a σ_A-weighted $2F_o - F_c$ map were deleted.

2.4. Structure and sequence analysis

Structural comparisons were made using *LSQMAN* (Kleywegt, 1999), *MAP* (Lu, 2000) and *DALI* (Holm & Sander, 1998). *STRIDE* (Frishman & Argos, 1995) was used for the definition of secondary-structure elements. Programs from the *PHYLIP* package (Felsenstein, 1989) were used to construct a neighbour-joining tree representation of structural similarities from *MAP*-derived data. From an initial tree containing all class I and class II PLA$_2$ crystal structures (except mutants and chemically modified proteins), very similar pairs of structures were identified and the lower resolution structure deleted. *BOBSCRIPT* (Esnouf, 1997) and *MOLSCRIPT*2 (Kraulis, 1991) were used to produce structural figures, while *ALSCRIPT* (Barton, 1993) was used to format alignments. *Xmgrace* (http://plasma-gate.weizmann.ac.il/Grace/) was used to plot graphs.

2.5. Enzyme assay

PLA$_2$ activity was measured using a previously described assay (Cho & Kézdy, 1991; Holzer & Mackessy, 1996) modified for 96-well plates. The standard assay mixture contained 200 µl buffer (10 mM Tris–HCl, 10 mM CaCl$_2$, 100 mM NaCl pH 8.0), 20 µl of the synthetic substrate 4-nitro-3-(octanoyloxy) benzoic acid, 20 µl water and 20 µl PLA$_2$ in a final volume of 260 µl. After addition of PLA$_2$ (20 µg), the mixture was incubated for up to 40 min at 310 K, with the absorbance being read at 10 min intervals. The enzyme activity, expressed as the initial velocity of the reaction (V_o), was calculated based on the increase in absorbance after 20 min for various substrate concentrations. All assays were performed in triplicate and the absorbances at 425 nm were measured using a SpectraMax 340 multiwell plate reader (Molecular Devices, Sunnyvale, CA, USA).

3. Results and discussion

3.1. Structure solution and refinement

Suitable structures to use in molecular replacement were determined using the *FFAS* program (Rychlewski *et al.*, 2000). For each, a model was built for the piratoxin III sequence (Toyama *et al.*, 1999) using the *MODELLER* program (Sali & Blundell, 1993). These five models were superimposed and used as input to *MOLREP* (Vagin & Teplyakov, 1997) by applying the NMR option. The use of multiple independent models can improve molecular-replacement results, particularly in difficult cases (*e.g.* Leahy *et al.*, 1992). *MOLREP* straightforwardly solved the molecular-replacement problem automatically. The correct rotation solution was positioned first with a rotation function/σ value of 9.55, compared with the next best scoring solution of 6.01. Using this rotation, the correct translation solution for the first molecule in the asymmetric unit had a correlation coefficient of 0.236 and an R factor of 54%. Placing of the second molecule resulted in a correlation coefficient of 0.360 and an R factor of 50%.

In order to determine which of the five models was the best basis for further refinement, the multiple MR solution was 'dissociated' into its five component models and each of these was subjected to rigid-body refinement followed by multiple torsion-angle simulated annealing in *CNS* (Brünger *et al.*, 1998). Ten different annealed structures were generated for each starting model. Comparison of these results clearly showed refined 1cl5-based models to be the best bases for further refinement (Table 2). Table 2 also shows the effectiveness of torsion-angle simulated annealing in combination with a maximum-likelihood refinement target, cross-validation (Rice & Brünger, 1994; Adams *et al.*, 1997) and strict NCS. A dramatic 12% reduction in R_{free} compared with the rigid-body refined model was achieved in a single step.

Solvent flattening was also employed and yielded significant improvements in map quality and interpretability. As refinement progressed, two regions of difference map density located in the binding sites of each monomer were convincingly modelled as 2-propanol molecules. 135 water molecules could be located during the final stages of refinement.

In the final model 44 of the 121 residues were exempted from the strong NCS restraints otherwise applied: residues 1–3, 10, 17, 19, 21–24, 27–33, 42, 45, 55–58, 60–61, 63, 66, 77–81,

106, 109, 111–114 and 116–120. With eight exceptions (residues 27–29, 45, 63, 66 and 80–81), these are involved in crystal contacts or are neighbours of crystal contacts.

During refinement, several mismatches between side chains corresponding to published piratoxin III sequences and electron density became apparent. The following corrections were made: Leu5→Phe, Gln7→Lys, Gly22→Val, Leu31→Gly, Tyr45→Phe, Lys48→Asp, Ala54→Leu, Gly56→Ser, Trp68→Arg, Leu71→Gly, Leu82→Arg, Leu85→Ile, Gly101→Asp, Arg108→Met, Tyr109→Ser, His110→Tyr and Pro113→Ser. This unusually high error rate for the protein primary sequence was confirmed by the sequencers (Marcos Toyama, personal communication). Information from homologous sequences was used to help determine the most likely correct residues at each position. A simulated-annealing omit map density for Met108–Tyr110 in subunit A of the final model is shown in Fig. 1. The presence of a small number of further sequence errors, particularly for residues with isosteric alternatives, cannot be ruled out. In the C-terminal region, the final model suggests the presence of an additional residue not present in the piratoxin III sequence. With the following residue numbers adjusted accordingly, this would lie between Lys117 and Ala119. The distance between Lys117 C and Ala119 N in subunit B, which would be covalently linked in the absence of an extra residue, is 4.71 Å. PLA$_2$ sequences in general show significant length variation in the C-terminal region. Database searches reveal the existence of many PLA$_2$ homologues with an extra residue at exactly this position (the most similar from *Agkistrodon halys pallas* with SWISS-PROT accession No. O42187), which is usually serine or threonine.

3.2. Description of the final model

The data in Tables 1 and 3 show a well refined structure with excellent stereochemistry. The structure is, for the most part, well defined by electron density (Fig. 2). The only significant regions of poorer definition, as seen in elevated B factors and poorer real-space correlation coefficients (Fig. 2), are the loop from residues 75 to 80 and the C-terminal region from position 110 onwards. Disorder prohibited the modelling of residue Asn78 in either subunit, the inferred residue 118 (see above) in either subunit and Ala119 in subunit A. In a Ramachandran plot (Laskowski *et al.*, 1993), 86.7% of residues are located in the most favoured areas, none in disallowed areas and just two in generously allowed areas. These, Leu114 in subunit B and Lys116 in subunit A, are reasonably well defined by density, albeit located in the C-terminal region with higher B factors (Fig. 2).
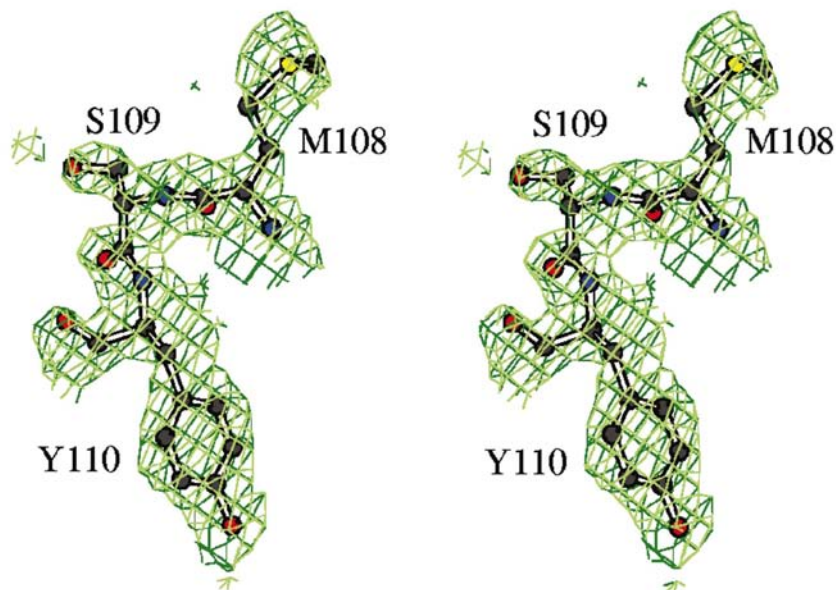

Figure 1
Stereo figure illustrating simulated-annealing omit map density for residues 108–110 in subunit A. Density in a σ_A-weighted $2F_o - F_c$ map, calculated after simulated annealing with the three residues omitted, is contoured at 1σ.
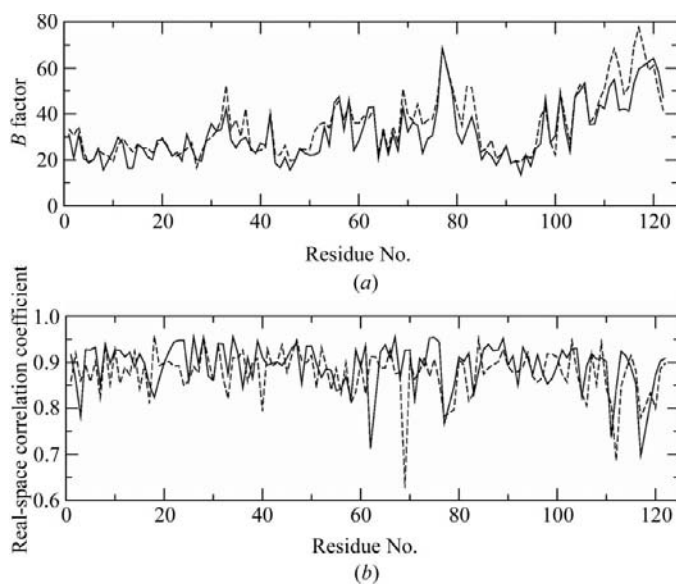

Figure 2
(*a*) Per-residue B factors (Å^2) and (*b*) real-space correlation coefficient for the final model. Solid lines are used for subunit A and dotted lines for subunit B.

The final model contains the now familiar three major helices in an almost parallel arrangement and the β-wing. A fourth shorter helix, sometimes defined in other crystal structures (*e.g.* Fig. 3), is not identified as such by *STRIDE* (Frishman & Argos, 1995) in the present structure owing to the disruptive effect of the *cis*-peptide bond preceding Pro19. Despite its proximity to the substrate-binding site, the variability in sequence and peptide-bond nature at position 19 seems to have no functional consequences.

The two 2-propanol molecules in the final model, one bound to each subunit, are well defined by density, with real-space

Table 3
Refinement statistics.

Values in parentheses are for the highest resolution shell.

No. of non-H protein atoms	1887
No. of non-H 2-propanol atoms	8
No. of non-H solvent atoms	135
Resolution range (Å)	14.7–2.4 (2.5–2.4)
No. of reflections	8166 (1046)
R (%)	20.1 (30.1)
R_{free} (%)	25.5 (36.5)
Mean temperature factor B (Å^2)	
All atoms	33.5
Protein	32.7
Main chain	30.7
Side chain	31.6
Subunit A	31.0
Subunit B	34.5
2-Propanol	48.4
Solvent	39.1
R.m.s. deviation from ideal values	
Bond lengths (Å)	0.007
Bond angles (°)	1.4

correlation coefficients of 0.83 and 0.80 and B factors of 48.1 and 48.7 Å^2, respectively. The trigonal pyramidal shape of 2-propanol means that its exact orientation in the density, if a single orientation indeed exists, cannot be determined; in no orientation is the O atom capable of hydrogen bonding to the protein. This situation is reminiscent of the cottonmouth snake venom K49 PLA$_2$ crystal structure in which density, also in the PLA$_2$ binding pocket, was interpreted as dioxane which, like the 2-propanol here, was present in the crystallization conditions (Holland *et al.*, 1990). In line with the absence of calcium in the crystallization conditions, no Ca^{2+} ions were assigned in the final model. The program *WASP* (Nayal & Di Cera, 1996) was used to confirm the absence of possible calcium ions among those assigned as water.

Despite nearly a third of residues disobeying the NCS relationship between subunits A and B, C$^\alpha$ differences for corresponding residues in the superposed subunits are less

than 1 Å, with the sole exception of the C-terminal region from residues 117–121 (Fig. 4).

3.3. Structural comparisons

For comparison of the model with other structures, the consensus PLA$_2$ numbering scheme introduced by Renetseder *et al.* (1985) will be used. Its relationship to piratoxin III numbering may be seen in Fig. 3.

Examination of the crystal lattice shows that a putative dimer can be identified with an interface resembling that observed in previous crystal structures involving the β-wing (*e.g.* da Silva Giotto *et al.*, 1998; Lee *et al.*, 2001; see Fig. 5). However, an alternative dimer structure can be identified with similarly favourable properties (Fig. 5). This alternative interface involves the C-terminal regions, the Ca^{2+}-binding loops and the two helices 2, which lie nearly parallel and whose contacts centre on Gly53. The carboxyl group of Gly33 on the radically reorganized Ca^{2+}-binding loop (see below) forms a hydrogen bond across the interface with Ser56 of the alternate subunit. Recent work shows that simple interface surface area is by far the most important consideration in predicting physiological dimers among crystal contacts between monomers (Valdar & Thornton, 2001). Calculations show that the isolated subunit B loses 516 Å^2 on formation of the conventional interface and 510 Å^2 on formation of the alternative interface. Similarly, shape-complementarity analysis (Lawrence & Colman, 1993) reveals near-identical values of 0.51 and 0.53, respectively. The B factors of the β-wing offer little help in choosing between possible dimers. In the conventional dimer structures, the B factors of the β-wing are depressed (*e.g.* da Silva Giotto *et al.*, 1998), in contrast to their elevation relative to the remainder of the structure in the monomeric enzyme structure (Arni *et al.*, 1999). In the present structure, the β-wing B factors, which are 31.9 and 37.4 in subunits A and B, respectively, are close to the overall B factor of 32.7. The general existence of flexibility of oligomerization in the PLA$_2$ family is illustrated by the trimer observed in crystals of Indian cobra phospholipase A$_2$ (Fremont *et al.*, 1993).

The result of a systematic subunit comparison of the present structure with other PLA$_2$s is shown in Fig. 6. Three main branches are evident in the tree. Two correspond to class I and class II PLA$_2$ enzymes (top and centre, respectively, in Fig. 6), while the third contains the vipoxin complex (PDB code 1aok; Perbandt *et al.*, 1997) and its isolated inhibitor chain (PDB code 1vpi; Devedjiev *et al.*, 1997).

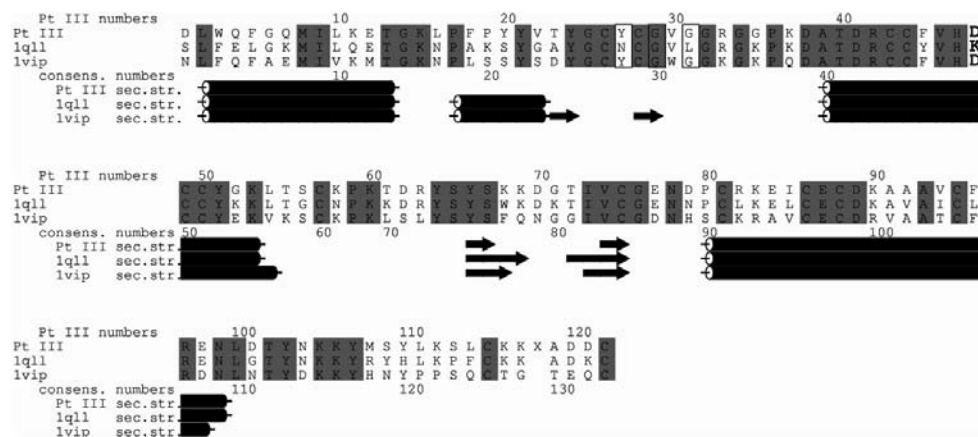The present structure is clearly positioned in the class II PLA$_2$

Figure 3
Alignment of piratoxin III with 1qll and 1vip. Piratoxin III numbering, as present in the PDB file, is shown above the alignment and the consensus numbering scheme introduced by Renetseder *et al.* (1985) is shown below the alignment. Secondary-structure elements were defined with *STRIDE* (Frishman & Argos, 1995). Conserved residues are shaded, residues whose main chain is involved in calcium binding are boxed and position 49, either Lys or Asp in the different PLA$_2$ classes, is in bold.

branch of the tree but, compared with the structures of that branch, is structurally divergent. Examination of the superposed class II structures reveals the main differences to lie in
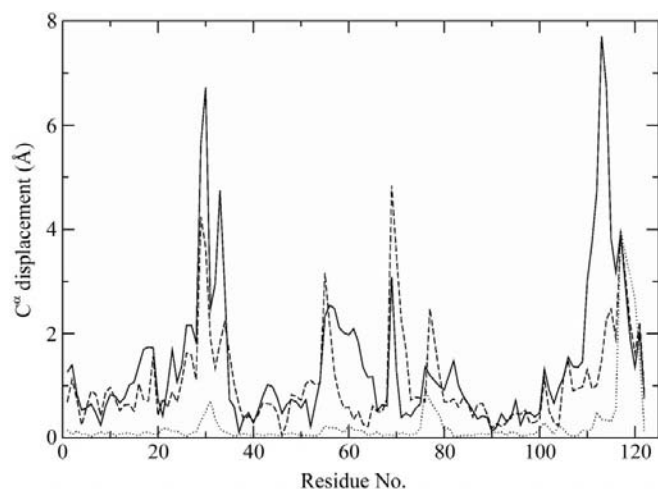

Figure 4
C^α displacements along the chain for subunit A of the present structure (dotted line), 1qll (solid line) and 1vip (dashed line) superimposed on subunit B.
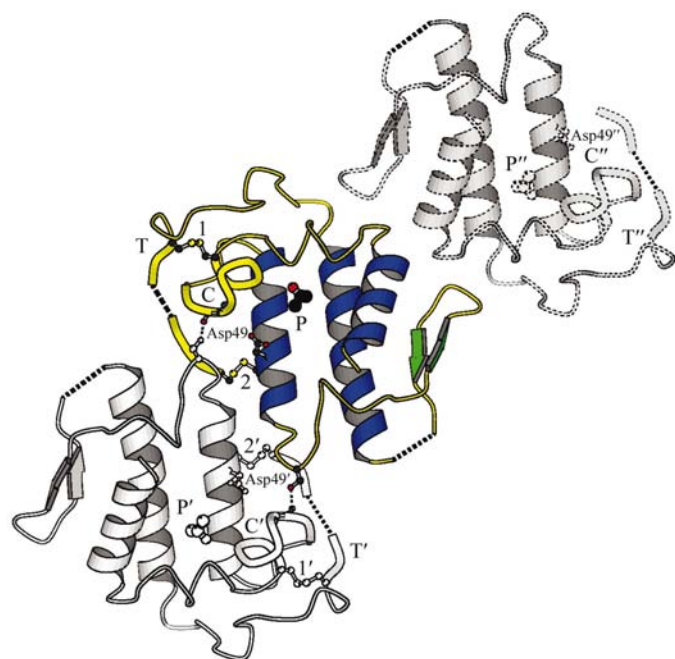

Figure 5
Possible dimer interfaces identified from analysis of crystal contacts. The 'conventional' dimer comprises the central coloured subunit and the dotted subunit (upper right). The 'alternative' dimer contains the central subunit and the white subunit (lower left). Helices, strands and coil of the central subunit are coloured blue, green and yellow, respectively. Thick dotted lines indicate parts of the structure for which density did not permit location of the model. The calcium-binding loop and C-terminal tail are drawn in broader coil and labelled C and T, respectively. The 2-propanol molecule occupying the hydrophobic part of the substrate-binding site is drawn and labelled P. Asp49 residues are drawn and labelled, as are two disulfide bonds linking the calcium-binding loop and the C-terminal tail, Cys27–Cys125 (labelled 1) and Cys50–Cys133 (labelled 2), mentioned in the text. The inter-subunit hydrogen bonds between Gly33–Ser56′ and Gly33′–Ser56 are represented by narrow dotted lines.

two regions of the chain; the Ca^{2+}-binding loop around residue 30 and the C-terminal region around residue 125. For the purposes of detailed comparisons, both chains of the present structure were compared with the structure of K49 piratoxin II (PDB code 1qll; Lee *et al.*, 2001) and the most similar D49 enzyme structure, that of the enzyme from *Vipera russelli russelli* (PDB code 1vip; Carredano *et al.*, 1998). The comparison is illustrated in Figs. 4 and 7.

While a degree of structural variability in both the Ca^{2+}-binding loop (in the absence of Ca^{2+}) and the C-terminal region is commonly noted in PLA_2 structures, the structural variation exhibited in the present structure is of a different order (Figs. 4 and 7). The binding of Ca^{2+}, required for phospholipase activity in D49 PLA_2s (Scott & Sigler, 1994), involves the main-chain carbonyl groups of residues 28, 30 and 32. In the Ca^{2+}-bound human enzyme (PDB code 1kvo; Cha *et al.*, 1996), the distance between Ca^{2+} and Gly30 O is 2.3 Å. From this same essentially invariant Ca^{2+} position, Gly30 O in 1vip (D49, calcium-free) is at a distance of 4.2 Å; Gly30 O in
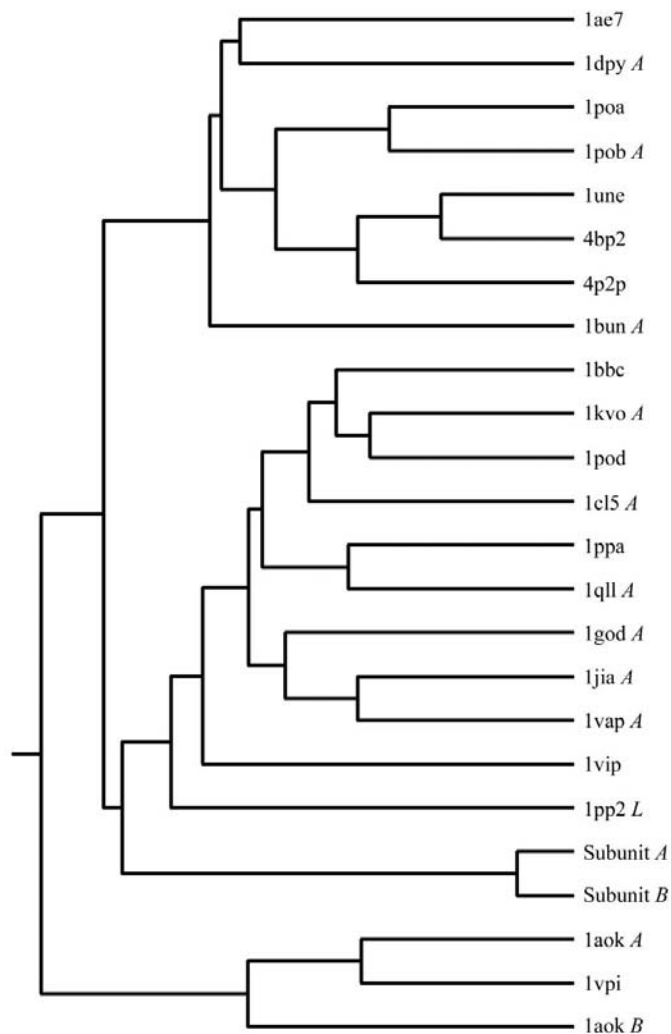

Figure 6
Neighbour-joining tree representation of structural relationships among PLA_2s. Distances between structures are calculated from their structural similarities as quantitated with *MAP* (Lu, 2000).
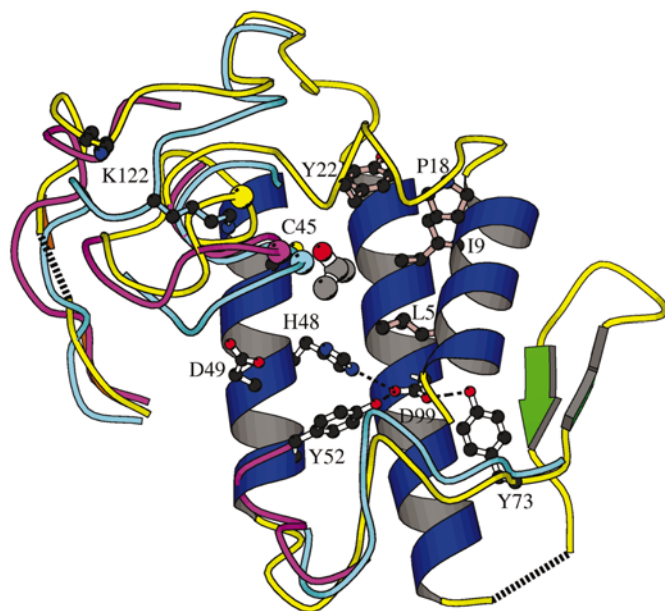
Figure 7
Schematic representation of the piratoxin III final model. Helices, strands and coil are coloured blue, green and yellow, respectively. In regions of significant structural difference, the superposed structures of 1qll (magenta) and 1vip (cyan) are drawn. The C^α atoms of Gly30 in the structures are drawn as spheres in the same colours. Catalytic residues (white bonds) and fatty-acid binding residues (Lee *et al.*, 2001; brown bonds) are shown in ball-and-stick representation, along with Lys122 in the present structure and in 1qll. The modelled position of 2-propanol in the present structure is drawn in a fatter ball-and-stick representation. Dotted lines in the backbone trace mark regions not defined by electron density. Dotted lines between catalytic residues indicated hydrogen bonds.

1qll (K49) is 4.0 Å away. The same measurement in the present structure yields 8.6 Å in subunit A and 8.3 Å in subunit B (see also Fig. 7). Clearly, the distortion of the calcium-binding loop in the present structure goes well beyond that expected to arise from the simple absence of calcium. The extreme diversion taken by the main chain at residues 30–31 seems to be associated with a change in the backbone dihedral angles of Cys29. In previous crystal structures, it occupies the β area of the Ramachandran plot, with typical φ, ψ values of around $-80, -120°$. In the new piratoxin III structure it is shifted to the α area, with φ, ψ angles of $-52, -57°$. This change is clearly defined by the electron-density maps (Fig. 2).

3.4. Functional aspects

Piratoxin III is known to possess the PLA_2 activity expected of a D49 member of the family (Soares *et al.*, 2001). Interestingly, using the synthetic non-micellar substrate 4-nitro-3-(octanoyloxy) benzoic acid (Holzer & Mackessy, 1996), the dependence of activity on substrate concentration is markedly sigmoidal (Fig. 8), with an $S_{0.5}$ value of around 28.4 mM and a Hill coefficient of 3.7. Classical Michaelis–Menten behaviour is more commonly reported for PLA_2s, but a number of other reports of sigmoidal rate substrate behaviour have appeared (Burke *et al.*, 1995; Beghini *et al.*, 2000).
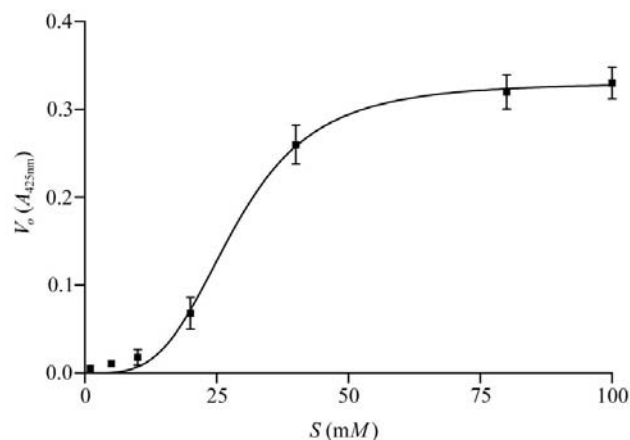

Figure 8
The dependence of initial PLA_2 rate (V_o) on substrate concentration (S). Measurements were made in triplicate. The data were fitted to the Hill equation, yielding a Hill constant of 3.7 and $S_{0.5}$ of 28.4 mM. The error bars mark standard deviations.

One common explanation for this behaviour would be the existence of both active and inactive structural conformations, the transition between which is influenced by substrate. Since the crystallized form would be unable to bind calcium and hence be catalytically inactive, it is tempting to regard it as an inactive T-state form and suppose that an active R-state can be induced by substrate binding. The R-state would more closely resemble existing crystal structures for other PLA_2 enzymes, with the canonical Ca^{2+}-binding loop structure (Lee *et al.*, 2001). Intriguingly, a dimer interface of the 'alternative' type observed in the crystal lattice (Fig. 5) would offer plausible routes of communication between active sites. The binding of phospholipid substrate to one site, with the phospho group interacting with bound Ca^{2+}, could readily influence the conformation of the Ca^{2+}-binding loop of that subunit. Through the disulfide bridge between Cys27 and Cys125, this signal could be transmitted to the C-terminal portion. The disulfide bridge between Cys50, the neighbour of the calcium-binding Asp49, and Cys133 offers an additional route for communication of a signal from substrate-binding site to the C-terminal tail. Both the Ca^{2+}-binding loop and C-terminal region contribute to the 'alternative' dimer interface (Fig. 5) so that conformational changes could readily be transmitted to the alternate dimer, conferring cooperative substrate on the enzyme. In the 'conventional' dimer structure, substrate binding occurs distant to the interface (Fig. 5), so that communication between subunits is not readily explained. The frustrating difficulty in determining the biologically relevant dimer interface, much as functional data must favour the 'alternative' type, should encourage further study of PLA_2s that show sigmoidal dependence of rate on substrate concentration, particularly the determination of holo- and apo-enzyme structures of the same enzyme.

research papers

References

Adams, P. D., Pannu, N. S., Read, R. J. & Brünger, A T. (1997). *Proc. Natl Acad. Sci. USA*, **94**, 5018–5023.

Arni, R. K., Fontes, M. R., Barberato, C., Gutierrez, J. M., Diaz, C. & Ward, R. J. (1999). *Arch. Biochem. Biophys.* **366**, 177–182.

Barton, G. J. (1993). *Protein Eng.* **6**, 37–40.

Beghini, D. G., Toyama, M. H., Hyslop, S., Sodek, L. C., Novello, J. C. & Marangoni, S. (2000). *J. Protein Chem.* **19**, 679–684.

Brünger, A. T. (1992). *Nature (London)*, **355**, 472–474.

Brünger, A. T., Adams, P. D., Clore, G. M., DeLano, W. L., Gros, P., Grosse-Kunstleve, R. W., Jiang, J. S., Kuszewski, J., Nilges, M., Pannu, N. S., Read, R. J., Rice, L. M., Simonson, T. & Warren, G. L. (1998). *Acta Cryst.* D**54**, 905–921.

Burke, J. R., Witmer, M. R., Tredup, J., Micanovic, R., Gregor, K. R., Lahiri, J., Tramposch, K. M. & Villafranca, J. J. (1995). *Biochemistry*, **34**, 15165–15174.

Carredano, E., Westerlund, B., Persson, B., Saarinen, M., Ramaswamy, S., Eaker, D. & Eklund, H. (1998). *Toxicon*, **36**, 75–92.

Cha, S. S., Lee, D., Adams, J., Kurdyla, J. T., Jones, C. S., Marshall, L. A., Bolognese, B., Abdel-Meguid, S. S. & Oh, B. H. (1996). *J. Med. Chem.* **39**, 3878–3881.

Cho, W. & Kézdy, F. J. (1991). *Methods Enzymol.* **197**, 75–79.

Collaborative Computational Project, Number 4 (1994). *Acta Cryst.* D**50**, 760–763.

Cowtan, K. D. & Zhang, K. Y. (1999). *Prog. Biophys. Mol. Biol.* **72**, 245–270.

Dessen, A., Tang, J., Schmidt, H., Stahl, M., Clark, J. D., Seehra, J. & Somers, W. S. (1999). *Cell*, **97**, 349–360.

Devedjiev, Y., Popov, A., Atanasov, B. & Bartunik, H. D. (1997). *J. Mol. Biol.* **266**, 160–172.

Dijkstra, B. W., Drenth, J., Kalk, K. & Vandermaalen, P. J. (1978). *J. Mol. Biol.* **124**, 53–60.

Esnouf, R. M. (1997). *J. Mol. Graph.* **15**, 132–134.

Felsenstein, J. (1989). *Cladistics*, **5**, 164–166.

Fremont, D. H., Anderson, D. H., Wilson, I. A., Dennis, E. A. & Xuong, N. H. (1993). *Proc. Natl Acad. Sci. USA*, **90**, 342–346.

Frishman, D. & Argos, P. (1995). *Proteins*, **23**, 566–579.

Gerrard, J. M., Robinson, P., Narvey, M. & McNicol, A. (1993). *Biochem. Cell Biol.* **71**, 432–439.

Gutierrez, J. M. & Lomonte, B. (1995). *Toxicon*, **33**, 1405–1424.

Holland, D. R., Clancy, L. L., Muchmore, S. W., Ryde, T. J., Einspahr, H. M., Finzel, B. C., Heinrikson, R. L. & Watenpaugh, K. D. (1990). *J. Biol. Chem.* **265**, 17649–17656.

Holm, L. & Sander, C. (1998). *Nucleic Acids Res.* **26**, 316–319.

Holzer, M. & Mackessy, S. P. (1996). *Toxicon*, **34**, 1149–1155.

Jones, T. A., Zou, J. Y., Cowan, S. W. & Kjeldgaard, M. (1991). *Acta Cryst.* A**47**, 110–119.

Keith, C., Feldman, D. S., Deganello, S., Glick, J., Ward, K. B., Jones, E. O. & Sigler, P. B. (1981). *J. Biol. Chem.* **256**, 8602–8607.

Kleywegt, G. J. (1999). *Acta Cryst.* D**55**, 1878–1884.

Kleywegt, G. J. & Brünger, A. T. (1996). *Structure*, **4**, 897–904.

Kleywegt, G. J. & Jones, T. A. (1996). *Acta Cryst.* D**52**, 829–832.

Kleywegt, G. J. & Jones, T. A. (1998). *Acta Cryst.* D**54**, 1119–1131.

Kraulis, P. J. (1991). *J. Appl. Cryst.* **24**, 946–950.

Laskowski, R. A., MacArthur, M. W., Moss, D. S. & Thornton, J. M. (1993). *J. Appl. Cryst.* **26**, 283–291.

Lawrence, M. C. & Colman, P. M. (1993). *J. Mol. Biol.* **234**, 946–950.

Leahy, D. J., Axel, R. & Hendrickson, W. A. (1992). *Cell*, **68**, 1145–1162.

Lee, W. H., da Silva Giotto, M. T., Marangoni, S., Toyama, M. H., Polikarpov, I. & Garratt, R. C. (2001). *Biochemistry*, **40**, 28–36.

Lloret, S. & Moreno, J. J. (1993). *Toxicon*, **31**, 949–956.

Lu, G. (2000). *J. Appl. Cryst.* **33**, 176–183.

Mancuso, L. C., Correa, M. M., Vieira, C. A., Cunha, O. A., Lachat, J. J., de Araújo, H. S., Ownby, C. L. & Giglio, J. R. (1995). *Toxicon*, **33**, 615–626.

Maraganore, J. M., Merutka, G., Cho, W., Welches, W., Kezdy, F. J. & Heinrikson, R. L. (1984). *J. Biol. Chem.* **259**, 13839–13843.

Matthews, B. W. (1968). *J. Mol. Biol.* **33**, 491–497.

Nayal, M. & Di Cera, E. (1996). *J. Mol. Biol.* **256**, 228–234.

Otwinowski, Z. (1993). *Proceedings of the CCP4 Study Weekend. Data Collection and Processing*, pp. 56–62. Warrington: Daresbury Laboratory.

Pan, H., Liu, X. L., Ou-Yang, L. L., Yang, G. Z., Zhou, Y. C., Li, Z. P. & Wu, X. F. (1998). *Toxicon*, **36**, 1155–1163.

Pannu, N. S. & Read, R. J. (1996). *Acta Cryst.* A**52**, 659–668.

Perbandt, M., Wilson, J. C., Eschenburg, S., Mancheva, I., Aleksiev, B., Genov, N., Willingmann, P., Weber, W., Singh, T. P. & Betzel, C. (1997). *FEBS Lett.* **412**, 573–577.

Polikarpov, I., Perles, L. A., de Oliveira, R. T., Oliva, G., Castellano, E. E., Garratt, R. & Craievich, A. (1998). *J. Synchrotron Rad.* **5**, 72–76.

Polikarpov, I., Teplyakov, A. & Oliva, G. (1997). *Acta Cryst.* D**53**, 734–737.

Read, R. J. (1986). *Acta Cryst.* A**42**, 140–149.

Renetseder, R., Brunie, S., Dijkstra, B. W., Drenth, J. & Sigler, P. B. (1985). *J. Biol. Chem.* **260**, 11627–11634.

Rice, L. M. & Brünger, A. T. (1994). *Proteins*, **19**, 277–290.

Rychlewski, L., Jaroszewski, L., Li, W. & Godzik, A. (2000). *Protein Sci.* **9**, 232–241.

Sali, A. & Blundell, T. L. (1993). *J. Mol. Biol.* **234**, 779–815.

Schevitz, R. W. *et al.* (1995). *Nature Struct. Biol.* **2**, 458–465.

Scott, D. L., Otwinowski, Z., Gelb, M. H. & Sigler, P. B. (1990). *Science*, **250**, 1563–1566.

Scott, D. L. & Sigler, P. B. (1994). *Adv. Protein Chem.* **45**, 53–88.

Shimohigashi, Y., Tani, A., Matsumoto, H., Nakashima, K. & Yamaguchi, Y. (1995). *J. Biochem.* **118**, 1037–1044.

Silva Giotto, M. T. da, Garratt, R. C., Oliva, G., Mascarenhas, Y. P., Giglio, J. R., Cintra, A. C., de Azevedo, W. F. Jr, Arni, R. K. & Ward, R. J. (1998). *Proteins*, **30**, 442–454.

Soares, A. M., Andriao-Escarso, S. H., Bortoleto, R. K., Rodrigues-Simioni, L., Arni, R. K., Ward, R. J., Gutierrez, J. M. & Giglio, J. R. (2001). *Arch. Biochem. Biophys.* **387**, 188–196.

Toyama, M. H., Costa, P. D., Novello, J. C., de Oliveira, B., Giglio, J. R., da Cruz-Hofling, M. A. & Marangoni, S. (1999). *J. Protein Chem.* **18**, 371–378.

Toyama, M. H., Soares, A. M., Wen-Hwa, L., Polikarpov, I., Giglio, J. R. & Marangoni, S. (2000). *Biochimie*, **82**, 245–250.

Tsai, I. H., Wang, Y. M., Au, L. C., Ko, T. P., Chen, Y. H. & Chu, Y. F. (2000). *Eur. J. Biochem.* **267**, 6684–6691.

Vagin, A. & Teplyakov, A. (1997). *J. Appl. Cryst.* **30**, 1022–1025.

Valdar, W. S. & Thornton, J. M. (2001). *J. Mol. Biol.* **313**, 399–416.

Verity, M. A. (1992). *Neurotoxicology*, **13**, 139–147.

Ward, R. J., Alves, A. R., Ruggiero Neto, J., Arni, R. K. & Casari, G. A (1998). *Protein Eng.* **11**, 285–294.